chemosensors

Article

Reading Dye-Based Colorimetric Inks: Achieving Color Consistency Using Color QR Codes

Ismael Benito-Altamirano [1,2,*], Laura Engel [3,4], Ferran Crugeira [5,6], Miriam Marchena [6], Jürgen Wöllenstein [3,4], Joan Daniel Prades [6,7] and Cristian Fàbrega [1]

1 MIND/IN2UB, Department of Electronics and Biomedical Engineering, Universitat de Barcelona, 08028 Barcelona, Spain; cfabrega@ub.edu
2 eHealth Center, Faculty of Computer Science, Multimedia and Telecommunications, Universitat Oberta de Catalunya, 08018 Barcelona, Spain
3 Fraunhofer Institute for Physical Measurement Techniques IPM, 79110 Freiburg, Germany
4 Department of Microsystems Engineering—IMTEK, University of Freiburg, 79110 Freiburg, Germany
5 Department of Chemistry, Universitat Autonoma de Barcelona, 08193 Bellaterra, Spain
6 ColorSensing, 08028 Barcelona, Spain
7 Laboratory for Emerging Nanometrology (LENA), Institute of Semiconductor Technology (IHT), Technische Universität Braunschweig, Hans-Sommer Str. 66, 38106 Braunschweig, Germany
* Correspondence: ismael.benito@ub.edu

Abstract: Color consistency when reading colorimetric sensors is a key factor for this technology. Here, we demonstrate how the usage of machine-readable patterns, like QR codes, can be used to solve the problem. We present our approach of using back-compatible color QR codes as colorimetric sensors, which are common QR codes that also embed a set of hundreds of color references as well as colorimetric indicators. The method allows locating the colorimetric sensor within the captured scene and to perform automated color correction to ensure color consistency regardless of the hardware used. To demonstrate it, a CO_2-sensitive colorimetric indicator was printed on top of a paper-based substrate using screen printing. This indicator was formulated for Modified Atmosphere Packaging (MAP) applications. To verify the method, the sensors were exposed to several environmental conditions (both in gas composition and light conditions). And, images were captured with an 8M pixel digital camera sensor, similar to those used in smartphones. Our results show that the sensors have a relative error of 9% when exposed with a CO_2 concentration of 20%. This is a good result for low-cost disposable sensors that are not intended for permanent use. However, as soon as light conditions change (2500–6500 K), this error increases up to $\epsilon_{\mathbf{20}}$ = 440% (rel. error at 20% CO_2 concentration) rendering the sensors unusable. Within this work, we demonstrate that our color QR codes can reduce the relative error to $\epsilon_{\mathbf{20}}$ = 14%. Furthermore, we show that the most common color correction, white balance, is not sufficient to address the color consistency issue, resulting in a relative error of $\epsilon_{\mathbf{20}}$ = 90%.

Keywords: colorimetric sensors; color consistency; color QR codes; color correction; machine-readable patterns

check for updates

Citation: Benito-Altamirano, I.; Engel, L.; Crugeira, F.; Marchena, M.; Wöllenstein, J.; Prades, J.D.; Fàbrega, C. Reading Dye-Based Colorimetric Inks: Achieving Color Consistency Using Color QR Codes. *Chemosensors* **2024**, *12*, 260. https://doi.org/10.3390/chemosensors12120260

Received: 8 November 2024
Revised: 6 December 2024
Accepted: 11 December 2024
Published: 13 December 2024

1. Introduction

Colorimetric indicators have been increasing their presence in the field of gas and environmental sensing in recent years [1–3]. This is likely due to their low cost, disposability, and ease of fabrication, as well as the increasing accessibility and ubiquity of color measurement technology, such as digital cameras in mobile phones. However, from a color measurement perspective, the variety of digital cameras in the market is too large [4]. This led to research into methods of how digital images could be captured as consistently as possible. This is the key aspect and the principal barrier in implementing this technology for daily use [5].

Several authors have tackled this problem, and we can divide their solutions into two major groups: those that try to fix the environmental conditions of the sensor capture and those that try to correct the capture using standard image processing techniques [6]. On the one hand, the authors presented a hardware extension for smartphone devices to obtain measurements from lateral-flow tests [7] used lab-on-a-chip solutions to perform the sensor readout [8] or employed low-cost commercial electronics [9]. On the other hand, the authors presented solutions to perform colorimetric readouts by placing color charts in the captured scene [10].

In this context, we have already proposed a way to integrate color charts and colorimetric indicators into one single machine-readable pattern, resembling a QR code [11], with no digital information but with the capacity to embed up two colorimetric sensors and up to 32 color references [12], which had to match with the color transition range of the sensor; later, we also presented a solution to embed up to 256 color references for two arbitrary chosen colorimetric dyes [13]. Recently, other authors have replicated similar solutions using a QR code (with digital information) that contains three sensors and only black and white pixels as color references [14]. And, in a more broad scope, it can be seen that there is "plenty of room" in QR codes to add layers of complexity to embed new features [15–17].

Now, we present our novel methodological approach using colorimetric dyes inside a machine pattern like before [13], but combined with digital data from our own standard, comprising back-compatible color QR codes. This is a machine-readable pattern that is back-compatible with the QR code standard and that allocates the color references and the colorimetric dyes to ensure proper color consistency for evaluation. Backward compatibility with the QR code standard allows the pattern to be read with any commercially available QR code scanner to obtain a URL or other message [18] (see Figure 1).

Figure 1. A Back-compatible Color QR Code [18] for the evaluation of colorimetric indicators. This QR code is read by commercial scanners and should display the URL: c-s.is/#38RmtGVV6RQSf (accessed on 12 December 2024) . It includes up to 125 reference colors, and the colorimetric dye is printed above the lower finder pattern, represented here as seven purple modules.

Regarding the colorimetric dyes, we used a carbon dioxide (CO_2) sensor, different from other applications that we tackled in previous works—e.g., detecting bad odor through ammonia, ammonia (NH_3), formaldehyde (CH_2O) and hydrogen sulfide (H_2S) detection [13]. This application is intended to monitor the gas concentration in Modified Atmosphere Packaging (MAP). In the food industry, it is common to package food under CO_2 and N_2 to increase the shelf life and ensure food freshness [5]. Moreover, we applied state-of-the-art color corrections methods [19] using the color references embedded in the color QR code. The color corrections used are affine [20], polynomial [21,22] and thin-plate spline corrections [23].

Results indicate that our colorimetric indicator presented a good sensor response in the green channel and responded linearly with the logarithm of the concentration. However, we also demonstrate that when the lightning conditions change, the apparent sensor becomes unfeasible to use due to color inconsistency if the capture is not properly corrected. This showed us that simple white-balance correction (the simplest affine color correction) is not enough to perform a proper colorimetric readout and that additional color references are needed. In that context, we demonstrate that our methodologic approach to embed the colorimetric dye with hundreds of color references is a good solution to achieve color-consistent readouts from handheld smartphones.

2. Materials and Methods

2.1. Sensor Fabrication

In previous research, we have already produced colorimetric indicators in several forms as soaked cellulose [24], using dip-coating [25] and screen-printing [13]. In terms of reproducibility, the screen-printing technology proved to be the most reliable of the methods. In addition, the technology can be seen as a starting point for the use of other printing technologies that are more suitable for mass production, such as gravure or flexographic printing [26].

The sensors were fabricated using a screen-printing machine of our facilities. The printing form was structured photomechanically with the pattern of the functional material at the respective location provided in the QR code pattern (see Figure 1). A polypropylene-coated white paper of 350 gr/m² was used for the prints. The back-compatible color QR codes, including digital information and color references, were previously printed using ink-jet technology. The sensor structure/layout is shown in Figure 2.

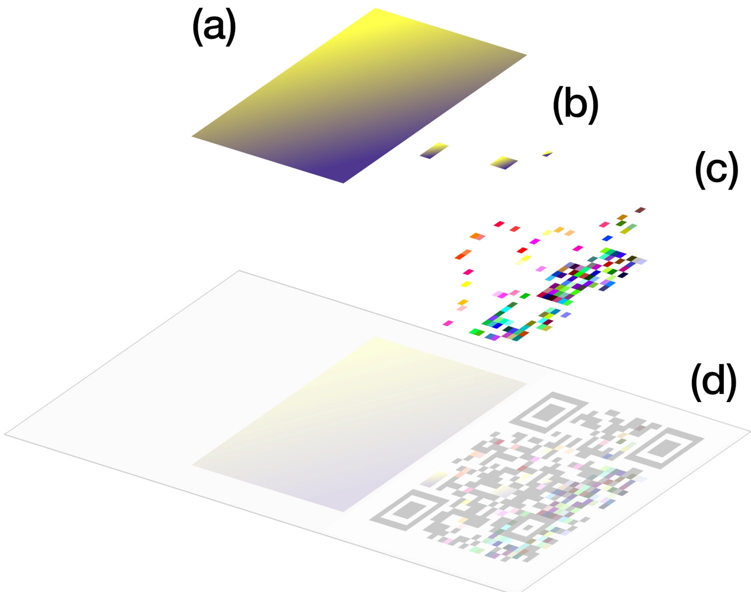

Figure 2. The structure of the color QR code from Figure 1: (**a**,**b**) Possible sensor inks placements. (**a**) Big sensor outside the QR code. (**b**) Smaller factor forms (3×2, 1×1, . . .) within the QR code. (**c**) Color references and how they are spread over the QR code area. (**d**) Whole sensor layout of the gas-sensitive color QR code.

The gas-sensitive material was formulated based on a sensor originally manufactured using ink-jet [27] printing and later adapted to screen printing. Qualitatively, the gas-sensitive layer is mainly based on a combination of *mCP* (meta-Cresol Purple) and *PR* (Phenol Red). It exhibits a color change from purple to yellow (see Figure 3) when exposed to CO_2.

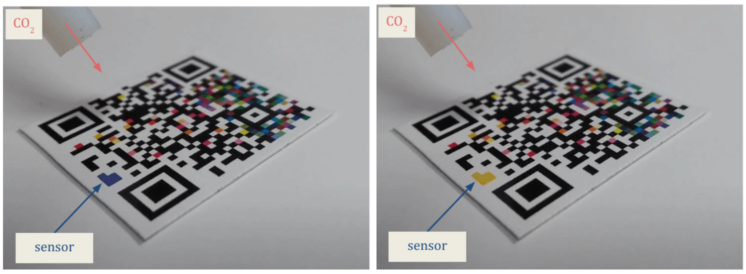

Figure 3. The sensor changes from purple to yellow when exposed to CO_2.

2.2. Experimental Conditions

The experimental setup used (see Figure 4) consists of the following three main subsystems: (1) a mass-flow control station, (2) a capture station and (3) a user station.

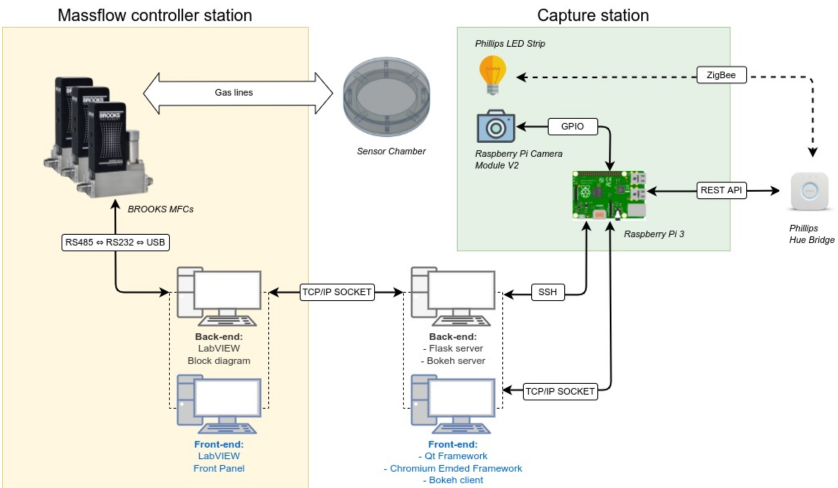

Figure 4. A mass-flow controller station, a capture station, and a user-access computer. The mass-flow controller station supplies a chamber in which the gas sensors are placed with modified atmospheres. The capture station takes time-lapse images of the sensor through an optical window of the chamber under controlled light settings. Finally, the user computer presents a web page interface to operate the system.

First, the *mass-flow control station* provided modified atmospheres to a chamber with an optical port where the gas sensors were placed. The MFC station was driven by BROOKS 5850S mass-flow controllers. The colorimetric indicator was exposed to a series of pulses of different controlled atmospheres, which were selected to tackle the scenario of a MAP application [5]. In total, the sensors were exposed to 15 gas pulses, each lasting 100 min. One pulse consisted of exposing the measurement chamber with the target gas CO_2, for 30 min, followed by a 70 min exposure to synthetic air (21% oxygen, 79% nitrogen) to return to a CO_2-free atmosphere state, with both states being exposed to a relative humidity of 40%. As a part of the experiment, five different gas concentrations were exposed to a total of three times: the actual atmospheres were measured and corrected following the manufacturer instructions [28] and are shown in Table 1.

Second, the *capture station* enabled to capture the colorimetric response of the sensor through the optical window of the chamber under controlled light conditions. The capture station was driven by several hardware components. Main components consisted of a Raspberry Pi 3B+–with a Raspberry Pi Camera v2–[29] and a RGB LEDs strip from Phillips Hue [30]. The sensor was exposed to different illumination conditions of white light: color temperatures between 2500 K and 6500 K were applied in steps of 500 K (see Figure 5). The camera settings were locked, without auto-exposition nor auto white balance, to capture consistent images across the entire dataset.

Table 1. Expected and measured CO_2 concentration for each gas pulse. The measured values were taken from the BROOKS instrumentation reading using a correction algorithm [28].

Pulse	Expected [%]	Measured [%]
1	20.0	25.21 ± 0.00
2	20.0	25.22 ± 0.22
3	20.0	25.22 ± 0.22
4	30.0	36.62 ± 0.22
5	30.0	36.67 ± 0.31
6	30.0	36.67 ± 0.31
7	35.0	42.10 ± 0.40
8	35.0	42.30 ± 0.40
9	35.0	42.20 ± 0.40
10	40.0	46.90 ± 0.40
11	40.0	47.30 ± 0.40
12	40.0	47.40 ± 0.40
13	50.0	57.60 ± 0.50
14	50.0	57.60 ± 0.50
15	50.0	57.60 ± 0.50

Figure 5. A printed sensor featuring a color QR code and two different colorimetric indicators (CO_2 indicator above, NH_3 below, which was not used in this experiment) inside the sensor chamber. The image shows the sensor before exposure to the target gas under three different light conditions: 2500 K (**left**), 4500 K (**middle**) and 6500 K (**right**).

Finally, the *user station* presented a web page interface to the user to operate the system. This station was implemented using Python (version 3.8): `flask` was used as a back-end service, and `bokeh` was used to present plots in the front-end.

2.3. Expected Response Model

For the following model, we expected the sensor response to be linear to the logarithm of the gas concentration [31]:

$$S[\%] = m \log(c) + n \tag{1}$$

where S is the colorimetric response of the sensor; c is the concentration of the target gas in the atmosphere; m and n are the constants of a linear law, where m represents the sensitivity towards the logarithm of the gas concentration; and n the response at very low gas concentrations.

The response $S[\%]$ is usually normalized following a metric. We defined this metric to resemble the normalization performed in an electronic gas sensor [31]. This kind of normalization divides the measured signal by the signal value assigned to the zero-gas concentration (sensor signal measured in synthetic air). This produces a metric that is not upper-bounded $[-1, \infty)$. The closer the initial "resistance" (color value) is to zero, the greater the response. Let us adapt this normalization for a red channel of a colorimetric indicator:

$$S_r[\%] = 100 \cdot \frac{r(c) - r_0}{r_0 - r_{ref}} \tag{2}$$

where S_r is the response in % of the red channel, c is the concentration of the target gas in %, $r(c)$ is the raw red sensor signal with an 8-bit resolution (0–255), r_0 is the value of $r(c = 0\%)$, and r_{ref} is an absolute color reference which acts as the "zero resistance" compared to electronic sensors. For our sensor, the value is $(r_{ref}, g_{ref}, b_{ref}) = (0, 0, 255)$ as the signal of the blue channel decreases while the signal of the red and green channels increases with the gas concentration [27].

Moreover, in this work, we wanted to recover the sensitivity as a function of the gas concentration using derivatives and thus calculate the error of the model for each gas concentration. To this end, we used error propagation rules:

$$\left.\frac{\Delta S}{\Delta c}\right|_c = \frac{m}{c} \Longrightarrow \Delta c|_c = \Delta S|_c \cdot \frac{c}{m} \tag{3}$$

where c is a given concentration recovered with the inverted (Equation (1)), m depends on each fitted model, $\Delta S|_c$ is the error of the measured signal response, and $\Delta c|_c$ is the model error for this given concentration. Relative errors were computed as

$$\epsilon_c = \frac{\Delta c|_c}{c} \cdot 100 \tag{4}$$

2.4. Color Correction Methods

We extracted the measured color values from the captured images using computer vision algorithms, relying on state-of-the-art libraries, to find the QR code features, e.g., finding, alignment and timing patterns [11]. Then, we subjected the color measures to several color correction methods [19].

Formally, these methods are based on the usage of color references used to compute color correction matrices. These matrices are applied to the captured RGB color space (r, g, b) to obtain a corrected RGB color space (r', g', b'). The main difference between the methods is the number of color references used to compute the correction matrix and the number of terms used to compute the matrix, as well as whether these terms are linear or non-linear with the (r, g, b) color space.

We selected several color correction methods based on previous work from authors [19], and we selected four variations for each group:

1. **Affine (AFF)**, with only linear terms [20];
2. **Vandermonde (VAN)**, with pure polynomial terms–i.e., r^2, g^2, b^2, …–[32];
3. **Cheung (CHE)**, with polynomial terms and cross-terms–i.e., rb^2, rg^2, …–[21];
4. **Finlayson (FIN)**, with root-polynomial terms–i.e., $\sqrt{r}$, $\sqrt{g}$, $\sqrt{b}$, …–[22];
5. **Thin-plate splines (TPS)**, with radial-basis functions–i.e., $r^2 \log(r)$, …–[23].

It is worth noting that the AFF group is the most common color correction method and forms the basis for all other groups. The AFF0 correction is defined as an affine color correction with only one reference, like a white-balance correction. The AFF1 is defined by two colors, black and white. All the other color corrections use the full set of 128 color references available in the color QR code. When fitting the color matrices, a Maximum Likelihood Estimator (MLE) method was used to adjust the color correction matrices [19].

3. Results and Discussion

After acquiring the color of the sensor under different environmental and light conditions, we computed the response of the sensors at 6500 K light conditions as it is the standard illuminant for the D65 color space. As expected, the indicator showed its largest difference in the green channel (Equation (2)) due to the color change from purple to yellow caused by the reaction with CO_2 [27]. We used this as the *ground-truth* response value to which responses under other light conditions (2500–6000 K) were compared. Before computing the response for each other light condition, we performed a color correction for each of the aforementioned color correction techniques.

Figure 6 shows the result of this process performed for a given color correction (TPS3), where all the pulses were overlapped into a signal pulse time frame (the pulse duration of min). The figure shows the response of the sensor captured under nine different illumination conditions after conversion into the D65 color space with three repetitions for each gas concentration. Our colorimetric indicator presents

- A fast response, achieving 90% of the $S_g(\%)$ response in less than 5 min for the highest concentration, and in less than 10 min for the lowest one;
- A reasonable maximum response above 150% for the higher target concentration of CO_2 50%;
- A slight saturation in the upper region of concentrations;
- Good reproducibility among the replicas of each pulse;
- A drift in the lower concentration area, as pulses did not end in the same response they started.

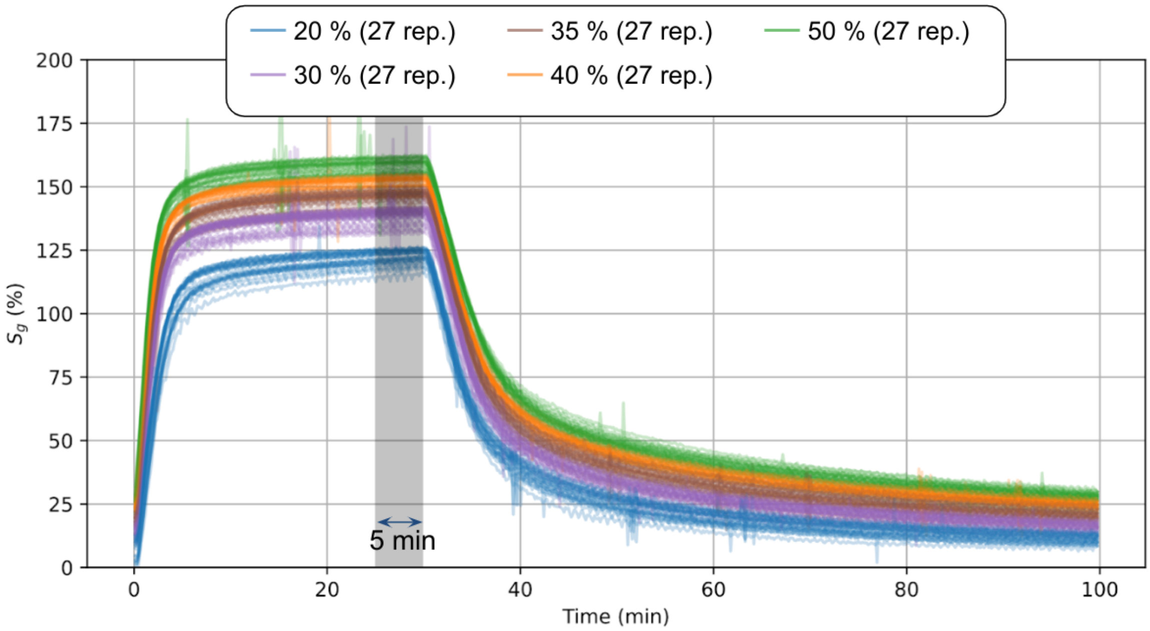

Figure 6. Response of the green channel under nine different light conditions (2500 K to 6500 K) with all pulses overlapped in the same time frame and after correction of the measured values using a color correction method. Each target gas concentration (20%, 30%, 35%, 40%, 50%) was exposed three times under the respective light condition, resulting in a total of 27 pulses for every gas concentration.

All in all, the sensor presented good characteristics to perform in a MAP application, regardless of a few properties that the sensor shows: saturation in the upper gas concentration range (50%) and drift in the lower range (0–5%) did not affect our further results as our models only aimed to fit the data of the range that applied to MAP (20–50%).

Based on these results, we selected a 5 min window to integrate the response of the sensor for each pulse (see Figure 6). These values represent the response of the sensor for each pulse in our model. We computed these values for each pulse and each color correction, and we added two reference cases to our results: (1) we studied the result with no correction being applied (NONE) and (2) we studied the result when the color correction was perfect (PERF). These references set the boundaries of worst- and best-case scenario, respectively. The PERF scenario is equal to the fit of the sensor response to the D65 illuminant and gives us information about the intrinsic error of the colorimetric indicator technology. The models were fitted accordingly to Equation (1), and the sensitivity Δc of the sensor and relative error ϵ_c were computed following Equation (3) and Equation (4), respectively.

Figure 7 shows a representation of the model fitting for the worst-case scenario (NONE). As expected, attempting to fit a model to raw data without color correction renders a meaningless fitting (low r^2), as opposed to fitting the model to the D65 illuminant data, which is the best-case scenario (PERF), which renders a perfect fitting (r^2 near 1).

The Δc and ϵ_c metrics for the NONE and PERF scenarios are displayed in Table 2. Under D65 illumination conditions (PERF), the sensor scored a relative error $\epsilon_c = 9\%$ at 20% of the CO_2 concentration and $\epsilon_c = 10\%$ at 50%. This is a good result for cost-effective disposable sensors, which are not meant to be persistent. However, when exposed to variable light conditions, the relative error increased up to 440–497% for the same gas concentration. This renders the sensors unusable.

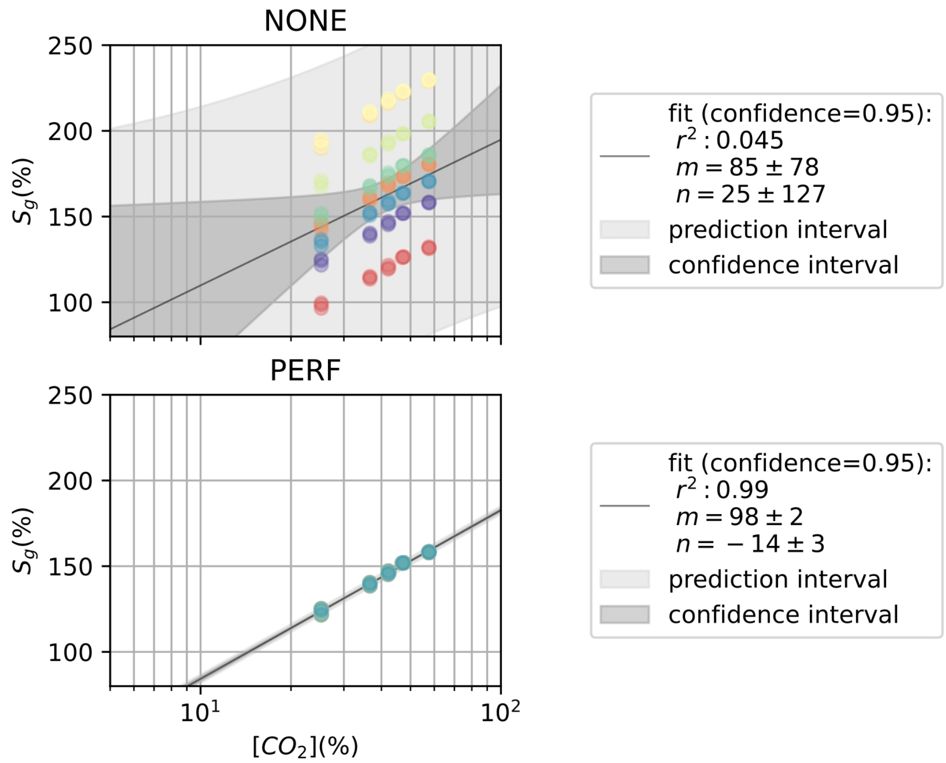

Figure 7. **Up**: Fitting the responses to a model without performing any color correction (NONE), which is the worst-case scenario, with different color in the data points indicating different illumination conditions and different transparency indicating different repetition sample. **Down**: Fitting the responses to a model for the ground-truth responses (PERF), which is the best-case scenario, where all color corrections recover the D65 color of the sensor perfectly.

Table 2 shows how the color correction techniques scored for a CO_2 concentration of 20% and 50%. On the one hand, the AFF0 and AFF1, which are white-balance implementations, only reduced the error to 90–102% and 68–77%, respectively. That demonstrated that a simple color correction it is not enough to perform a correct readout of a colorimetric sensor. On the other hand, AFF3 was the best correction method, scoring a relative error of 14–16%.

Non-linear techniques performed poorly in this scenario: the VAN and CHE methods (polynomial) scored closely to AFF3 relative errors from 17% to 21%. The FIN methods (root-polynomial) scored the worst results in the set ranging from 37% to 52%. And, the TPS (splines) achieved slightly worse results than AFF3, ranging from 22% to 33%. This demonstrated that the quantity of color references rather than the complexity of the colorimetric algorithm is important for this colorimetric problem.

Table 2. Summary of the obtained results. The summary includes metrics for each color correction for 8 different metrics: the first 3 (m, n, r^2) refer to the training model found; r^2_{valid} is the validation score of our models; $\mathbf{\Delta c_{20}}[\%]$ and $\mathbf{\Delta c_{50}}[\%]$ are the model resolution in concentration, with $c = 20\%$ and $c = 50\%$, respectively; $\epsilon_{50}[\%]$ and $\epsilon_{20}[\%]$ are their respective relative error, computed as $\mathbf{100} \cdot \frac{\Delta_c}{c}$.

Correction	$m\left[\frac{\%}{\%}\right]$	n [%]	$r^2[-]$	$r^2_{valid}[-]$	$\Delta c_{20}[\%]$	$\Delta c_{50}[\%]$	$\epsilon_{20}[\%]$	$\epsilon_{50}[\%]$
NONE	90 ± 80	200 ± 130	0.04	0.00	88	249	440	497
PERF	98 ± 2	-14 ± 3.0	0.99	0.99	2	5	9	10
AFF0	101 ± 19	-17 ± 31	0.56	0.10	18	51	90	102
AFF1	100 ± 14	-16 ± 23	0.69	0.45	14	38	68	77
AFF2	98 ± 10	-16 ± 16	0.81	0.34	10	27	48	55
AFF3	100 ± 3	-19 ± 5	0.98	0.97	3	8	14	16
VAN0	109 ± 4	-31 ± 6	0.97	0.96	3	10	17	19
VAN1	109 ± 4	-30 ± 7	0.97	0.97	4	11	19	21
VAN2	107 ± 4	-28 ± 6	0.97	0.97	3	10	17	20
VAN3	106 ± 4	-26 ± 6	0.97	0.97	4	10	18	20
CHE0	101 ± 4	-20 ± 6	0.97	0.94	3	9	17	19
CHE1	103 ± 4	-25 ± 6	0.98	0.97	3	9	16	18
CHE2	105 ± 4	-25 ± 6	0.97	0.97	3	9	17	19
CHE3	109 ± 4	-32 ± 6	0.97	0.96	3	10	17	20
FIN0	108 ± 4	-29 ± 7	0.97	0.95	4	11	19	21
FIN1	97 ± 8	-15 ± 12	0.88	0.62	7	21	37	42
FIN2	104 ± 8	-23 ± 13	0.88	0.77	8	22	38	43
FIN3	98 ± 9	-15 ± 15	0.83	0.35	9	26	46	52
TPS0	102 ± 6	-19 ± 9	0.94	0.97	5	15	27	31
TPS1	102 ± 5	-20 ± 9	0.95	0.97	5	14	26	29
TPS2	103 ± 6	-22 ± 10	0.92	0.88	6	17	30	33
TPS3	105 ± 5	-25 ± 8	0.95	0.94	4	13	22	25

4. Conclusions

This study demonstrates how one of the major challenges to widespread implementation of colorimetric sensors can be overcome. Following the studied example, a CO_2 colorimetric indicator for a MAP application that presented good reproducibility and responded linearly with the logarithm of the concentration was unusable due to the color consistency problem when a readout was performed under different ambient light conditions. In this context, we observed an increase in the relative error from 9 to 14% to 440–497% for the gas concentration range ($[CO_2] = 20$–50%) examined. A relative error of 9% represents a good result for cost-effective disposable sensors, which are not meant to be persistent. In comparison, for example, the commercially available electronic CO_2 sensor from Sensirion [33] has a 3% relative error.

All in all, we have demonstrated that the usage of references with only one or two colors [14] is not sufficient to solve the color consistency problem. Researchers must apply correction with an oversampling of color references of the color space of the indicator. At this point, an approach like ours, which uses color QR codes [18] to embed hundreds of color references as well as the colorimetric dyes themselves, is a good solution to solve the color consistency problem.

Moreover, a generic affine color correction was found to be sufficient to solve the color consistency problem. This is a linear color correction, like a white balance but with hundreds of color references [20]. This color correction method (AFF3) outperformed the other methods, including more high-order color corrections, such as the spline color corrections, which often tackle the problem better for open solutions, like correcting an entire image and not a single color patch [23].

Finally, future work could include the following topics: (1) More complex illumination configurations. This could change how the color corrections are performed in the model fittings. As with extreme light conditions, non-linear methods are expected to increase their performance. (2) Fine-tuning the camera capturing settings, as a similar way to change the environmental settings in the capture process. (3) Introduction of more locally bounded color references for specific problems, rather than using a predefined general set of color references.

Author Contributions: Conceptualization, I.B.-A. and J.D.P.; methodology, L.E., F.C. and M.M.; software, I.B.-A.; validation, L.E., F.C. and M.M.; formal analysis, I.B.-A. and C.F.; investigation, I.B.-A. and L.E.; resources, C.F. and J.D.P.; data curation, I.B.-A.; writing—original draft preparation, I.B.-A.; writing—review and editing, J.W., J.D.P. and M.M.; visualization, I.B.-A. and L.E.; supervision, J.W., J.D.P. and C.F.; project administration, C.F.; funding acquisition, J.W. and J.D.P. All authors have read and agreed to the published version of the manuscript.

Funding: This research work was funded by the Eurostars programs: "E! 11453 SnapGas" (Sensotran, S.L., Scemtec Transponder Technology GmbH, Universitat de Barcelona and Fraunhofer IPM) and "E! SnapFresh" (Sensotran, S.L., ColorSensing, S.L., Scemtec Transponder Technology GmbH and Fraunhofer IPM). I. Benito-Altamirano acknowledges the support from project PID2022-138721NB-I00, funded by MCIN (Spain). J.D. Prades acknowledges the support from the sponsorship of the Alexander von Humboldt Professorship of the Humboldt Foundation and the Federal Ministry for Education and Research (Germany). C. Fàbrega acknowledges the support from Agència per la Competitivitat de l'Empresa (ACCIO, Innotec 2021 ACE034/21/000057).

Institutional Review Board Statement: Not applicable.

Informed Consent Statement: Nor aplicable.

Data Availability Statement: The raw data supporting the conclusions of this article will be made available by the authors on request.

Conflicts of Interest: Authors Ferran Crugeira and Miriam Marchena were employed by the company ColorSensing SL. The remaining authors declare that the research was conducted in the absence of any commercial or financial relationships that could be construed as a potential conflict of interest.

References

1. Schmitt, K.; Tarantik, K.R.; Pannek, C.; Wöllenstein, J. Colorimetric Materials for Fire Gas Detection—A Review. *Chemosensors* **2018**, *6*, 14. [CrossRef]
2. Wang, Y.; Wang, X.; Ma, W.; Lu, R.; Zhou, W.; Gao, H. Recent developments in rhodamine-based chemosensors: A review of the years 2018–2022. *Chemosensors* **2022**, *10*, 399. [CrossRef]
3. Wu, Y.; Feng, J.; Hu, G.; Zhang, E.; Yu, H.H. Colorimetric sensors for chemical and biological sensing applications. *Sensors* **2023**, *23*, 2749. [CrossRef] [PubMed]
4. Yadav, P.; Yadav, L.; Laddha, H.; Agarwal, M.; Gupta, R. Upsurgence of smartphone as an economical, portable, and consumer-friendly analytical device/interface platform for digital sensing of hazardous environmental ions. *Trends Environ. Anal. Chem.* **2022**, *36*, e00177. [CrossRef]
5. Luo, X.; Zaitoon, A.; Lim, L.T. A review on colorimetric indicators for monitoring product freshness in intelligent food packaging: Indicator dyes, preparation methods, and applications. *Compr. Rev. Food Sci. Food Saf.* **2022**, *21*, 2489–2519. [CrossRef]
6. Fernandes, G.M.; Silva, W.R.; Barreto, D.N.; Lamarca, R.S.; Gomes, P.C.F.L.; da S Petruci, J.F.; Batista, A.D. Novel approaches for colorimetric measurements in analytical chemistry—A review. *Anal. Chim. Acta* **2020**, *1135*, 187–203. [CrossRef]
7. Long, K.D.; Woodburn, E.V.; Le, H.M.; Shah, U.K.; Lumetta, S.S.; Cunningham, B.T. Multimode smartphone biosensing: The transmission, reflection, and intensity spectral (TRI)-analyzer. *Lab Chip* **2017**, *17*, 3246–3257. [CrossRef]
8. Soda, Y.; Bakker, E. Quantification of colorimetric data for paper-based analytical devices. *ACS Sens.* **2019**, *4*, 3093–3101. [CrossRef]
9. Driau, C.; Fàbrega, C.; Benito-Altamirano, I.; Pfeiffer, P.; Casals, O.; Li, H.; Prades, J.D. How to implement a selective colorimetric gas sensor with off the shelf components? *Sens. Actuators B Chem.* **2019**, *293*, 41–44. [CrossRef]
10. Idros, N.; Chu, D. Triple-indicator-based multidimensional colorimetric sensing platform for heavy metal ion detections. *ACS Sens.* **2018**, *3*, 1756–1764. [CrossRef]

11. *ISO ISO/IEC 18004:2015*; Information Technology—Automatic Identification and Data Capture Techniques—QR Code Bar Code Symbology Specification. International Organization for Standardization: Geneva, Switzerland, 2015.
12. Benito-Altamirano, I.; Pfeiffer, P.; Cusola, O.; Daniel Prades, J. Machine-Readable Pattern for Colorimetric Sensor Interrogation. *Proceedings* **2018**, *2*, 906. [CrossRef]
13. Engel, L.; Benito-Altamirano, I.; Tarantik, K.R.; Dold, M.; Pannek, C.; Prades, J.D.; Wöllenstein, J. Printable Colorimetric Sensors for the Detection of Formaldehyde in Ambient Air. *ECS Meet. Abstr.* **2020**, *MA2020-01*, 2029. [CrossRef]
14. Escobedo, P.; Ramos-Lorente, C.E.; Ejaz, A.; Erenas, M.M.; Martínez-Olmos, A.; Carvajal, M.A.; García-Núñez, C.; de Orbe-Payá, I.; Capitán-Vallvey, L.F.; Palma, A.J. QRsens: Dual-purpose Quick Response code with built-in colorimetric sensors. *Sens. Actuators B Chem.* **2023**, *376*, 133001. [CrossRef]
15. Liu, T.; Yan, B.; Pan, J.S. Color visual secret sharing for QR code with perfect module reconstruction. *Appl. Sci.* **2019**, *9*, 4670. [CrossRef]
16. Chou, K.C.; Wang, R.Z. Dual-Message QR Codes. *Sensors* **2024**, *24*, 3055. [CrossRef] [PubMed]
17. Benito-Altamirano, I.; Crugeira, F.; Marchena, M.; Prades, J.D. The Application of Back-Compatible Color QR Codes to Colorimetric Sensors. *Proceedings* **2024**, *97*, 3. [CrossRef]
18. Benito-Altamirano, I.; Martínez-Carpena, D.; Casals, O.; Fábrega, C.; Waag, A.; Prades, J.D. Back-compatible Color QR Codes for colorimetric applications. *Pattern Recognit.* **2023**, *133*, 108981. [CrossRef]
19. Benito-Altamirano, I.; Martínez-Carpena, D.; Lizarzaburu-Aguilar, H.; Ventura, C.; Fàbrega, C.; Prades, J.D. Image color consistency in datasets: The Smooth-TPS3D method. *arXiv* **2024**, arXiv:2409.05159.
20. Finlayson, G.; Hordley, S.; Xu, R. Convex programming colour constancy with a diagonal-offset model. In Proceedings of the IEEE International Conference on Image Processing 2005, Genova, Italy, 14 September 2005. [CrossRef]
21. Cheung, V.; Westland, S.; Connah, D.; Ripamonti, C. A comparative study of the characterisation of colour cameras by means of neural networks and polynomial transforms. *Color. Technol.* **2004**, *120*, 19–25. [CrossRef]
22. Finlayson, G.D.; MacKiewicz, M.; Hurlbert, A. Color Correction Using Root-Polynomial Regression. *IEEE Trans. Image Process.* **2015**, *24*, 1460–1470. [CrossRef]
23. Menesatti, P.; Angelini, C.; Pallottino, F.; Antonucci, F.; Aguzzi, J.; Costa, C. RGB color calibration for quantitative image analysis: The "3D Thin-Plate Spline" warping approach. *Sensors* **2012**, *12*, 7063–7079. [CrossRef]
24. Fernández, L.; Pons, A.; Monereo, O.; Benito-Altamirano, I.; Xuriguera, E.; Casals, O.; Fàbrega, C.; Waag, A.; Prades, J.D. NO_2 Measurements with RGB Sensors for Easy In-Field Test. *Proceedings* **2017**, *1*, 471. [CrossRef]
25. Schmitt, K.; Tarantik, K.; Pannek, C.; Benito-Altamirano, I.; Casals, O.; Fàbrega, C.; Romano-Rodríguez, A.; Wöllenstein, J.; Prades, J.D. Colorimetric sensor for bad odor detection using automated color correction. In *SPIE Proceedings*; Fonseca, L., Prunnila, M., Peiner, E., Eds.; SPIE: Bellingham, WA, USA, 2017. [CrossRef]
26. Leach, R.; Leach, R.; Pierce, R. *The Printing Ink Manual*; Springer: Berlin/Heidelberg, Germany, 1993.
27. Zhang, Y.; Lim, L.T. Inkjet-printed CO_2 colorimetric indicators. *Talanta* **2016**, *161*, 105–113. [CrossRef] [PubMed]
28. Brooks Instruments. *Brooks® Smart-Series Digital Mass Flow Meters and Controllers—Models 5800-S*; Brooks Instrument: Hatfield, PA, USA, 2008.
29. Pagnutti, M.; Ryan, R.E.; Cazenavette, G.; Gold, M.; Harlan, R.; Leggett, E.; Pagnutti, J. Laying the foundation to use Raspberry Pi 3 V2 camera module imagery for scientific and engineering purposes. *J. Electron. Imaging* **2017**, *26*, 013014. [CrossRef]
30. Cusano, C.; Napoletano, P.; Schettini, R. Evaluating color texture descriptors under large variations of controlled lighting conditions. *J. Opt. Soc. Am. A* **2016**, *33*, 17. [CrossRef]
31. Engel, L.; Benito-Altamirano, I.; Tarantik, K.R.; Pannek, C.; Dold, M.; Prades, J.D.; Wöllenstein, J. Printed sensor labels for colorimetric detection of ammonia, formaldehyde and hydrogen sulfide from the ambient air. *Sens. Actuators B Chem.* **2021**, *330*, 129281. [CrossRef]
32. Kalman, D. The Generalized Vandermonde Matrix. *Math. Mag.* **1984**, *57*, 15–21. [CrossRef]
33. Sensirion. *Datasheet Sensirion SCD30 Sensor Module—CO_2, Humidity, and Temperature Sensor*; Version 0.94; Sensirion: Stäfa, Switzerland, 2019.